Improving cryo-EM maps by resolution-dependent and heterogeneity-aware deep learning

Hong Cao, Tao Li, Ji Chen, Jiahua He[1,*], and Sheng-You Huang[2,*]

School of Physics, Huazhong University of Science and Technology, Wuhan, Hubei 430074, P. R. China

Key Words: Cryo-EM, Cryo-ET, Post-processing, Map improvement, Deep learning

[1]Current address: Department of Biochemistry and Biophysics, University of California San Francisco, San Francisco, California, USA.

[2]Lead contact

[*]e-mail: jiahua.he@ucsf.edu (J.H.), huangsy@hust.edu.cn (S.-Y.H.)

Abstract

Cryo-electron microscopy (cryo-EM) has emerged as a leading technology for determining the structures of biological macromolecules. However, map quality issues such as noise and loss of contrast hinder accurate map interpretation. Traditional and deep learning-based post-processing methods offer improvements but face limitations particularly in handling map heterogeneity. Here, we present EMReady2, a substantial evolution of our previously developed deep learning-based methodology, towards a generalist model for improving cryo-EM maps. EMReady2 introduces a local resolution-dependent training strategy, allowing it to effectively address map heterogeneity. Additionally, EMReady2 extends its applicability to cryo-EM maps with nucleic acids, intermediate-resolution maps, and cryo-electron tomography (cryo-ET) maps. Extensive evaluations on diverse test sets of 94 maps at 2.0–10.0 Å resolutions demonstrate that EMReady2 is a universally applicable post-processing model for improving EM density maps in terms of both quality and interpretability, and significantly outperforms existing methods. EMReady2 is freely available at http://huanglab.phys.hust.edu.cn/EMReady2/.

1 Introduction

The rapid development of hardware[1], sample preparation[2] and image processing algorithms[3–6] has positioned cryo-EM as one of the mainstream technologies for elucidating structural basis of biological molecules as well as the interactions among them[7–9]. In order to build accurate atomic models of biological macromolecules using cryo-EM[10–20], the quality and interpretability of the reconstructed three-dimensional (3D) density maps is critical. However, owing to radiation damage, particle flexibility, preferred orientation, and reconstruction error, the original reconstructed 3D density maps often suffer from a high level of background noise, loss of contrast at high frequencies, as well as heterogeneity of resolution across the map[21–23], which pose significant obstacles for accurate structural interpretation.

To reduce these defects and improve the quality of cryo-EM density maps, various post-processing algorithms have been developed, which can be broadly categorized into two classes: traditional methods[24–29] and deep learning-based methods[30–32]. Traditional approaches to map post-processing are often performed in the Fourier domain of density maps, where Fourier coefficients/amplitudes at different frequencies are re-weighted to enhance contrast and reduce noise. Leveraging the advancements in deep learning algorithms and their proven efficacy in image restoration tasks, several deep learning-based post-processing methodologies have been developed recently[30–32]. Unlike traditional map sharpening methods, deep learning-based post-processing directly modifies the input map in real space, offering the advantage of leveraging complex, data-driven models to accurately capture and enhance underlying structural details while maintaining the ability of contrast enhancement and noise reduction.

DeepEMhancer[30], which employs a 3D UNet deep learning architecture, mimics the local sharpening effect of LocScale[25]. EM-GAN[31], which adopts the concept of adversarial learning, modifies the input density map to achieve minimized differences between the output map and an ideal simulated map at the voxel level. While DeepEMhancer and EM-GAN have achieved notable successes

in handling experimental cryo-EM maps, they face distinct challenges. Deepemhancer's performance is severely restricted by the performance of its learning target, LocScale, while EM-GAN's focus on voxel-level differences may miss important details for structural context. To address the limitations of existing deep learning-based post-processing methods, our prior research introduced an innovative approach, EMReady[32]. EMReady adopts the 3D Swin-Conv-UNet (SCUNet) architecture[33], which learns the mapping from experimental primary maps processed by traditional sharpening methods to ideal maps simulated from atomic models by simultaneous local and non-local deep learning. It has been demonstrated in practical scenarios that EMReady can effectively enhance the quality of cryo-EM density maps, and thus facilitate more accurate interpretations[34–37].

Despite the cutting-edge performance of EMReady, several significant challenges remain to be addressed for better performance in realistic applications. Firstly, EMReady generates its target simulated map by applying a uniform resolution across the entire structure. This approach can lead to significant biases in simulated maps due to poorly modeled regions within the reference structures, consequently diminish the performance of the trained model. The other consequence of using a uniform resolution is that the trained model tends to apply density modification with the same strength to different regions across the map during inference, which may fail to accommodate the inherent heterogeneity present in experimental cryo-EM maps, and thus result in suboptimal modifications across the map. Secondly, the development of EMReady mainly focused on cryo-EM maps for proteins, which severely limits its application on maps with nucleic acids. Due to higher dynamics of nucleic acids, the quality of density for nucleic acids is often lower than that for proteins on cryo-EM maps. This makes enhancing the density quality of nucleic acids in cryo-EM maps crucial for accurate structure-based analysis of biological processes, especially for maps of protein-nucleic acid complex where the heterogeneity between proteins and nucleic acids should be taken into consideration. Thirdly, EMReady was mainly designed for maps with near-atomic resolutions, it may not be as effective for intermediate-resolution maps. Lastly, EMReady's training and evaluation were conducted exclusively on the maps by cryo-EM single-particle analysis (SPA). As cryo-ET plays an increasingly vital

role in elucidating biological processes, it is crucial to also handle cryo-ET subtomogram averaging (STA) maps. Overall, in light of these issues, there is a pressing need to improve EMReady's robustness against map heterogeneity, and to extend its methodology to effectively process cryo-EM maps containing nucleic acids, intermediate-resolution maps and cryo-ET maps.

Meeting the need, we take a significant leap from EMReady towards a universally applicable deep learning-based method of map post-processing, evolving our methodology into EMReady2. To improve the robustness of EMReady2 to map heterogeneity, we now target local resolution-dependent simulated maps, where local resolution is characterized by the atomic Q-score of the PDB structure versus its experimental map[38]. As such, the biases introduced by poorly modeled regions are mitigated during the training process, and the trained model is able to tailor its density modification tactics in different map regions in a heterogeneity-aware manner during inference. Moreover, the training and evaluation of EMReady2 is expanded to encompass maps containing nucleic acid molecules, intermediate-resolution maps, and cryo-ET maps. We extensively evaluate EMReady2 on three diverse test sets of cryo-EM and cryo-ET maps at 2.0–10.0 Å resolutions for proteins and/or nucleic acids. The evaluation results demonstrate that EMReady2 achieves significant improvements over existing methods including its predecessor, EMReady.

2 Results and Discussion

2.1 Overview of EMReady2

Figure 1 shows an overview of EMReady2. The density map post-processing workflow of EMReady2 is illustrated in Fig. 1**a**. The input to EMReady2 is one single EM density map. EMReady2 supports maps derived from both cryo-EM SPA and cryo-ET STA, which can contain proteins, nucleic acids, and their complexes. The input density map is first chunked into a series of overlapping volume slices. These volume slices are then fed into a 3D SCUNet[33] to obtain the corresponding processed slices.

Finally, the slices processed by the network are re-assembled to yield the output map.

The training workflow of EMReady2 is illustrated in Fig. 1**d**. A non-redundant set of experimental maps obtained from the Electron Microscopy Data Bank (EMDB)[39] is used as the training set. The corresponding atomic structures of these maps are taken from the Protein Data Bank (PDB)[40]. For each pair of atomic structure and its corresponding density map in the training set, Q-scores[38], which indicate the local resolvability of the experimental density map, are calculated based on the atomic structure. The simulated density map is then generated using different local resolution values derived from the Q-scores for different atoms. The experimental map and its corresponding simulated map are chunked into pairs of volume slices. In each training step, experimental volume slices are processed by the network and then compared to the simulated slices, which serve as the learning target. A loss function combining smooth L1 loss and structural similarity (SSIM) L2 loss is used to iteratively optimize the network through backpropagation.

2.2 Evaluations on nucleic acid-included maps

To access the capability of EMReady2 on improving both protein and nucleic acid densities in EM maps, we first evaluate the performance of EMReady2 on the test set of 18 cryo-EM SPA primary maps that contain nucleic acids and compare it with DeepEMhancer, phenix.auto_sharpen and EMReady. Here, five different metrics are used to measure the performance: unmasked map-model FSC-0.5, CC_box, CC_mask, CC_peaks[41], and Q-score[38].

As shown in Fig. 2**a**, in terms of unmasked map-model FSC-0.5, EMReady2 achieves an average value of 4.18 Å, significantly improved from 5.70 Å for the deposited maps, 4.94 Å for DeepEMhancer, 5.70 Å for phenix.auto_sharpen, and 4.59 Å for EMReady (Table 1). Figure 2**b** shows the average Q-scores of different methods. On average, EMReady2 achieves the highest average Q-score of 0.501, compared to 0.453 for deposited maps, 0.368 for DeepEMhancer, 0.446 for phenix.auto_sharpen, and 0.458 for EMReady (Table 1). We further analyze the distribution and cu-

mulative distribution of Q-scores on nucleic acid atoms. As shown in Fig. 2**c**, EMReady2 generally achieves improved Q-scores on nucleic acid atoms. Figure 2**d**,**e**,**f** shows the average map-model correlation coefficients (CC_box, CC_mask, and CC_peaks). Specifically, the average CC_box, CC_mask, and CC_peaks values for the maps processed by EMReady2 are 0.883, 0.786, and 0.765, respectively, which are substantially higher than 0.820, 0.765, and 0.706 for the deposited maps (Table 1). Considering all the evaluation metrics, EMReady and EMReady2 are both capable of improving from the deposited primary map, and significantly outperform DeepEMhancer and phenix.auto_sharpen. Furthermore, EMReady2 achieves a superior performance to EMReady, indicating the effectiveness of including local quality information and nucleic acid data during training.

Figure 2**g** shows an example of EMD-9105, a 3.6 Å cryo-EM map for the group II intron retroelement prior to DNA integration. It can be seen from the figure that EMReady2 effectively improves the density traces for the double-helix strands. Furthermore, after being processed by EMReady2, the density signals become distinguishable for teh base pairs, which is not achieved by other methods including EMReady. Quantitatively, the EMReady2-processed map achieves an improved Q-score of 0.606, which is significantly higher than 0.553 for the deposited map, 0.450 for DeepEMhancer, 0.549 for phenix.auto_sharpen, and 0.564 for EMReady. EMReady2 also achieves the highest unmasked map-model FSC-0.5 of 3.02 Å, CC_box of 0.917, CC_mask of 0.852, and CC_peaks of 0.848. Figure 2**f** shows an enlarged view of the protein-nucleic acid interface of another example, EMD-33983, a 3.36 Å cryo-EM map for CasPi with guide RNA and target DNA. It is can be seen from the figure that EMReady2 is the only method that can simultaneously improve the densities for both protein and nucleic acids, despite the severe heterogeneity between them. All the other methods yield almost unchanged and even worse density signals for nucleic acids, while EMReady2 successfully recovers the density traces for the nucleotide chain. Specifically, the unmasked map-model FSC-0.5 and Q-score for the EMReady2-processed map are 3.16 Å and 0.520, respectively, which are considerably higher than 4.17 Å and 0.488 for the deposited map.

2.3 Evaluations on intermediate-resolution maps

Despite the highest resolution that EM technique can reach is being continuously improved, owing to the intrinsic dynamics of some biological systems, it is expected that an innegligible portion of structures will still only be solved at intermediate resolutions. To evaluate the general applicability of EMReady2 on intermediate-resolution maps, we compare its performance with existing methods on a set of 58 cryo-EM maps at intermediate resolutions (i.e., 4.0–8.0 Å).

As shown in Fig. 3**a**, EMReady2 significantly improves the unmasked map-model FSC-0.5 of the deposited map, and outperforms all of the other post-processing methods. EMReady2 successfully improves FSC-0.5 for 57 out of the 58 deposited maps in the test set. On average, EMReady2 achieves an FSC-0.5 of 6.36 Å, compared to 7.63 Å for the deposited maps, 7.11 Å for DeepEMhancer, 7.63 Å for phenix.auto_sharpen, and 6.63 Å for EMReady (Table 2). In addition to FSC-0.5, the Q-scores of EMReady2-processed maps are also significantly improved (Fig. 3**b**). EMReady2 achieves an average Q-score of 0.331, compared with 0.313 for deposited maps, 0.203 for DeepEMhancer, 0.307 for phenix.auto_sharpen, and 0.314 for EMReady (Table 2). Furthermore, EMReady2 is also capable of improving CC_box, CC_mask, and CC_peaks. The maps processed by EMReady2 achieve average CC_box, CC_mask, and CC_peaks values of 0.838, 0.696, and 0.633, respectively, which are significantly higher than 0.770, 0.672, and 0.558 for the depostied map (Table 2), and those of the other post-processing approaches including EMReady. (Fig. 3**c**–**e**). Specifically, out of the 58 maps in the test set, EMReady2 improves the CC_box for 51 maps, improves the CC_mask for 42 maps, and improves the CC_peaks for 49 maps.

Figure 3**f**,**g** shows an example of EMD-28000, a 5.6 Å cryo-EM map of Initial DNA-lesion (AP) binding by XPC and TFIIH complex2. The unmasked map-model FSC curve shown in Fig. 3**f** demonstrates that along a wide range of spatial frequencies, EMReady2 achieves the most effective enhancement among all of the methods. Comparison of the density maps shown in Fig. 3**g** reveals that the EMReady2-processed map provides greater clarity and connectivity in both protein and nucleic

acid densities, compared to the deposited map and the maps processed by other methods. Correspondingly, the map processed by EMReady2 achieves an improved unmasked FSC-0.5 and Q-score of 4.39 Å and 0.310, respectively, compared to 7.12 Å and 0.285 for the deposited primary map. Additionally, the EMReady2-processed map yields improved CC_box, CC_mask, and CC_peaks of respectively 0.874, 0.781, and 0.744, which are significantly higher than 0.746, 0.729, and 0.618 for the deposited map.

2.4 Evaluations on cryo-ET STA maps

Besides SPA, another important phase of EM-based technique is cryo-ET, which can also result in density maps of sub-nanometer resolutions by applying STA. We further evaluate the performance of EMReady2 on the test set of 18 cryo-ET STA maps, and compare it with DeepEMhancer, phenix.auto_sharpen, and EMReady. Since most of the cryo-ET STA maps in the test set only contain partial modeled regions, we select masked map-model FSC-0.5, Q-score, and CC_mask as the evaluation metrics.

As shown in Fig. 4**a**, the EMReady2-processed maps achieve the highest average masked map-model FSC-0.5 of 6.32 Å, compared to 7.06 Å for deposited maps, 6.83 Å for DeepEMhancer, 6.92 Å for phenix.auto_sharpen, and 6.45 Å for EMReady (Table 3). As illustrated in Fig. 4**b**, except for EMReady2, the other methods are not able to improve the CC_mask from deposited primary maps. The EMReady2-processed maps achieve an improved average CC_mask of 0.689, compared to 0.673 for the deposited maps (Table 3). Figure 4**c** shows the results of average Q-score. It can be seen from the figure that EMReady2 achieves an average Q-score of 0.392, compared with 0.361 for deposited maps, 0.280 for DeepEMhancer, 0.364 for phenix.auto_sharpen, and 0.378 for EMReady (Table 3). Figure 4**d** shows the distribution and cumulative distribution of the Q-scores for all atoms in the test set. Owing to the generally lower quality of STA maps, a significant proportion of atoms have low Q-scores of around 0.1 in the deposited map. However, after being processed by EMReady2, the

Q-score distribution of atoms shows significant shift towards higher values.

Figure 4**e** shows an example of EMD-12487, a 4.3 Å STA map of the mature RSV CA lattice. As illustrated in the figure, it is evident that only the EMReady- and EMReady2-processed maps can effectively denoise the deposited maps. Further comparison between EMReady2 and EMReady shows that EMReady2 can better preserve the regions with weak density signals, indicating the advantage of EMReady2 over EMReady when dealing with map heterogeneity. Quantitatively, EMReady2-processed map achieves higher unmasked map-model FSC-0.5, Q-score, and CC_mask of respectively 4.33 Å, 0.561, and 0.814 than 4.41 Å, 0.535, and 0.780 for the deposited primary maps, and 4.25 Å, 0.551, and 0.790 for the EMReady-processed maps. Figure 4**f** shows another example, EMD-14617, a 3.8 Å cryo-ET STA map of Rubisco from Cyanobium carboxysome. It can be observed from the figure that the density signals in the maps processed by EMReady and EMReady2 clearly shows the backbone trajectory of the PDB model, while the other methods fail to achieve this. Detailed comparison between EMReady2 and EMReady reveals that the map processed by EMReady2 exhibits a more continuous density trace for the backbone, especially for the loops. Correspondingly, the map processed by EMReady2 achieves improved unmasked FSC-0.5, Q-score, and CC_mask values of 4.15 Å, 0.469, and 0.806, respectively, compared with 5.18 Å, 0.432, and 0.759 for the deposited primary maps, and 4.31 Å, 0.459, and 0.776 for the EMReady-processed maps.

2.5 Improvement in map interpretability

The true enhancement of density map quality should improve the quality of the built models, or namely enhance the interpretability of the maps. Therefore, we conduct further analysis to assess the impact of EMReady2 in model building. To ensure unbiased results, we utilize phenix.map_to_model for automatic building of atomic models from the map regions segmented within 4.0 Å from each of the 111 chains in our first test set of 18 cryo-EM SPA maps with nucleic acids. The built models are compared with the deposited PDB structures through phenix.chain_comparison, from which two

metrics are reported: residue coverage and sequence recall.

The evaluation results on the test set are shown in Fig. 5**a**–**d** and are summarized in Table 4. Notably, EMReady2 significantly improves the residue coverage of the built atomic models with average values of 69.44% for proteins and 68.32% for nucleic acids, which are considerably higher than 56.60% and 45.11% for the deposited maps, 50.82% and 39.54% for DeepEMhancer, 57.36% and 50.18% for phenix.auto_sharpen, and 66.95% and 57.56% for EMReady. For sequence recall, EMReady2 achieves 28.60% for proteins and 24.57% for nucleic acid, which are much higher than 15.36% and 19.39% for the deposited maps and the other methods. The primary enhancement in EMReady2 compared to EMReady lies in the nucleic acid domains, which can be attributed to the incorporation of nucleic acid data and heterogeneity information during its training.

Figure 5**e** compares the modeling results for chains I and J of 6R25 (EMD-4710). It can be seen from the figure that EMReady2 effectively enhances the density traces for the DNA double helix, and thus results in a better-built model. Specifically, the model built on the EMReady2-processed map achieves a residue coverage of 77.90% and a sequence recall of 19.05%, respectively, compared with only 19.70% and 5.77% for the deposited maps. Figure 5**f** shows the modeling results for chain E of 6R25. Comparison of the loop regions indicates substantial improvements made by EMReady2 that lead to improved model building. On the EMReady2-processed map, the built model achieves a residue coverage and a sequence recall of 87.90% and 71.13%, respectively, which are much better than 60.60% and 4.06% for the model built on the deposited map.

2.6 Robustness of EMReady2 against map heterogeneity

Intrinsic flexibility in different part of the target molecule, preferred orientation of the particles on the grid, or errors in the subsequent image analysis, can lead to heterogeneity in the reconstructed EM density maps[21–23]. Here, we carry out detailed analysis of how EMReady2 deal with the maps with heterogeneity.

Figure 6**a**–**c** shows the example of EMD-33428, a 3.01 Å cryo-EM map of Native Tetrahymena ribozyme. It is shown that the deposited map exhibits an obvious heterogeneity of signals between protein and nucleic acid (Fig. 6**a**). Among the maps processed by different methods, EMReady2 shows the highest robustness against map heterogeneity. EMReady2 not only effectively enhances the high-resolution protein densities, but also rescues some lower-resolution signals for nucleic acids. Comparison between the local resolution maps calculated by MonoRes[21] for the deposited map and the EMReady2-processed map (Fig. 6**b**) indicates that EMReady2 can to some extent mitigate the heterogeneity of the density map. The FSC curve displayed in Fig. 6**c** also demonstrates that EMReady2 is able to enhance the signals along a broad range of spatial frequencies.

Figure 6**d**,**e** shows another example, EMD-20501, a 4.03 Å cryo-EM map of the human NatE/HYPK complex. As can be seen from the comparison, EMReady2 significantly enhances the entire map including the weaker density signal at the bottom part of the map. The angular distribution of local directional resolution measured by MonoDir[22] indicates a strong angular anisotropy in the deposited map, which is consistent with its heterogeneity of local resolution. After being processed by EMReady2, the heterogeneity in local resolution and angular resolution can be effectively mitigated, as shown in Fig. 6**e**.

3 Discussion

In this study, we have advanced our previously developed method, EMReady, to EMReady2, a universally applicable deep learning-based post-processing method for EM density maps. During training, we generate the target simulated map using varying local resolution values derived from Q-scores for different atoms within the structure. This mitigates training biases introduced by poorly modeled regions and allows the model to adapt its density modification strategies in a heterogeneity-aware manner during inference. Furthermore, our training and evaluation now encompass maps containing nucleic acid molecules, intermediate-resolution maps, and cryo-ET maps.

We have conducted comprehensive evaluations of EMReady2 on three diverse test sets covering different types of maps at 2–10 Å, and compared it with existing methods, including DeepEMhancer, phenix._auto_sharpen, and EMReady. The evaluation results demonstrate that EMReady2 significantly outperforms existing methods. EMReady2 can enhance the quality of maps for both proteins and nucleic acids. Also, EMReady2 shows effectiveness in enhancing maps across a wide range of resolutions, from 2 to 10 Å. Moreover, EMReady2 can be applied to the maps reconstructed not only by cryo-EM SPA but also by cryo-ET STA. We also demonstrate that EMReady2 improves the map interpretability in terms of *de novo* model building and is robust to map heterogeneity. These results confirm that EMReady2 fully meets the general requirements of EM map post-processing and aids in structural interpretation. EMReady2 is anticipated to serve as an enormously valuable tool in the workflow of EM-based structural and cell biology.

4 Methods

4.1 Data collection

In this study, all EM density maps and the corresponding atomic structures in our dataset are downloaded from the EMDB[39] and the PDB[40], respectively. To build a consensus and high-quality dataset that covers different types of EM density maps, all maps and PDB structures that meet the following criteria are collected: (i) resolution between 2.0–10.0 Å; (ii) reconstructed by single-particle analysis (SPA) or subtomogram averaging (STA); (iii) a unique correspondence between structure and density map; (iv) without any unknown atom/residue; (v) the total number of $C\alpha$ and $C4'$ atoms falls within the range of 20–2000; (vi) cross-correlation coefficient calculated by UCSF Chimera[42] between the structure and the density map is greater than 0.6; (vii) CC_mask calculated by phenix.map_model_cc[41] between the structure and the density map is greater than 0.5. Further manual inspection is conducted to exclude maps that exhibit obvious inconsistencies with the associated

PDB model from our dataset.

To remove the redundancy in our dataset, we use MMseqs2[43] to cluster the samples in our dataset by using a coverage and a sequence similarity thresholds of respectively 0.8 and 0.3 for proteins and 0.8 and 0.8 for nucleic acids. The clustering results in a non-redundant set of 507 maps, which are then divided into 348 training samples, 65 validation samples, and 94 testing samples. We further divide the test samples into three test sets targeting different evaluation purposes. The first test set is for cryo-EM SPA maps containing nucleic acids, including 18 maps at 2–7 Å resolutions. For each map in this test set, we ensure that more than 10% of residues in its corresponding PDB structure belong to nucleic acids. The second test set is for intermediate-resolution cryo-EM maps, which consists of 58 maps with resolutions ranging from 4.0 to 8.0 Å. The third test set comprises of 18 cryo-ET STA maps at 3–10 Å resolutions. To evaluate the improvement of map interpretability by EMReady2, we extract all of the 111 chains in our first test set, including 74 protein chains and 37 nucleic acid chains.

4.2 Generation of local resolution-dependent simulated maps

For each sample in the training set, the corresponding training objective, i.e., simulated map, is generated from its associated PDB structure. In stead of applying a uniform resolution across the entire structure, we covert the PDB structure to the simulated map in a heterogeneity-aware manner. Specifically, for each atom in the PDB structure, the Q-score is calculated using UCSF chimera[42]. Then, for i-th atom in the structure, the equivalent resolution $R_i^{\mathrm{Q-score}}$ can be derived from its Q-score as follows,

$$R_i^{\mathrm{Q-score}} = \begin{cases} \dfrac{q_i - 1.119}{-0.178}, & \text{if } i \in \text{protein}, \\ \dfrac{q_i - 0.997}{-0.138}, & \text{if } i \in \text{nucleic acid}, \end{cases} \tag{1}$$

where q_i denotes the Q-score for the i-th atom. Here, the mapping from Q-score to the equivalent resolution is taken from the original paper of Q-score, which was derived through linear regression on two sets of maps[38]. By combining the global resolution and the equivalent resolutions derived

from Q-scores, the final local resolutions for each of the atoms in the structure can be calculated by the following formula,

$$R_i^{\text{local}} = w \times R^{\text{global}} + (1 - w) \times R_i^{\text{Q-score}} \tag{2}$$

where R_i^{local} denotes the local resolution of the i-th atom, R_i^{global} denotes the global resolution (reported resolution) of the density map, and w is a weighting factor to balance the contribution from Q-score-derived resolution and the global resolution to the final local resolution.

Given a PDB structure of N atoms, the density value ρ on grid point $\mathbf{x}$ of the simulated map is calculated as follows,

$$\rho(\mathbf{x}) = \sum_{i=1}^{N} C_i Z_i \exp^{-k_i \|\mathbf{x} - \mathbf{r}_i\|^2} \tag{3}$$

where Z_i and $\mathbf{r}_i$ are the atomic number and the position vector of the i-th heavy atom ($i = 1, 2, \ldots, N$), respectively. k_i and C_i are derived from the local resolution, i.e., $k_i = \left(\pi/(0.6 + 0.8 \times R_i^{\text{local}})\right)^2$ and $C_i = (k_i/\pi)^{1.5}$. The value of w (0.8 in this study) is determined through a grid search to optimize the cross-correlation coefficient between the simulated map and the PDB structure calculated by UCSF Chimera on our training set, within the range of [0, 1.0] and with a step size of 0.1.

4.3 Network training

To train the network of EMReady2, we first unify the grid size of all maps in the training set to 1.0 Å through cubic interpolation. Next, the density values of each map are clipped to the range of 0 to the 99.999-percentile of the entire map, and then scaled to the range of 0 to 100. Finally, each pair of experimental and simulated maps is segmented into a series of pairs of volume slices using a sliding window of shape $60 \times 60 \times 60$ and a sliding stride of 30. Non-positive volume slices are excluded in order to ensure effective training.

EMReady2 employs Swin-Conv-Unet[33] as its network architecture for post-processing EM density maps. The network consists of three encoder, one bottleneck, and three decoder swin-conv (SC) blocks with skip connections. EMReady2 is implemented using PyTorch 2.0.0[44]. Data augmentation

is applied during training. Namely, the input pairs of volume slices are augmented by random 90° rotations, followed by randomly cropping a smaller slice of shape $48 \times 48 \times 48$ from the original slice of shape $60 \times 60 \times 60$.

The input of our network is density slices of shape $48 \times 48 \times 48$ with a grid interval of 1.0 Å. The outputs of our network are post-processed density slices of the same size. A combination loss function is adopted by EMReady2 to measure the difference between the output post-processed volume slices and the target simulated slices. This loss function consists of two terms. One is the smooth L1 loss, which is more sensitive to local differences of density values. The other is the structural similarity (SSIM) loss, which reflects the non-local correlation of density slices. Given a post-processed volume slice Y^{pred} and its corresponding simulated volume Y^{GT} of shape $M \times M \times M$ ($M = 48$ in this study), the smooth L1 loss is given as follows,

$$\mathcal{L}^{\text{SmoothL1}} = \frac{1}{M^3} \sum_{i=1}^{M} \sum_{j=1}^{M} \sum_{k=1}^{M} l(Y^{\text{pred}}_{i,j,k}, Y^{\text{GT}}_{i,j,k}) \tag{4}$$

where $l(Y^{\text{pred}}_{i,j,k}, Y^{\text{GT}}_{i,j,k})$ is the smooth L1 distance between the post-processed volume slice and the simulated volume slice at position (i, j, k). The smooth L1 distance is defined as follows,

$$l(a, b) = \begin{cases} 0.5 \times (a - b)^2, & \text{if } |a - b| < 1.0, \\ |a - b| - 0.5, & \text{otherwise.} \end{cases} \tag{5}$$

The SSIM Loss measures the contrast and structural similarity between the post-processed and the simulated volume slices, which is given as follows,

$$\mathcal{L}^{\text{SSIM}} = 1 - \frac{2\sigma_{Y^{\text{pred}}Y^{\text{GT}}} + \epsilon}{\sigma^2_{Y^{\text{pred}}} + \sigma^2_{Y^{\text{GT}}} + \epsilon} \tag{6}$$

where $\sigma_{Y^{\text{pred}}}$ and $\sigma_{Y^{\text{GT}}}$ are the standard deviations of the post-processed volume slice and the simulated volume slice, respectively, $\sigma_{Y^{\text{pred}}Y^{\text{GT}}}$ is the covariance between two slices, and $\epsilon = 1e - 6$ is introduced to prevent division by zero. By combining the smooth L1 loss and the SSIM loss, the final loss function used to train EMReady2 can be expressed as follows,

$$\mathcal{L}(Y^{\text{pred}}, Y^{\text{GT}}) = \mathcal{L}^{\text{SmoothL1}}(Y^{\text{pred}}, Y^{\text{GT}}) + \beta \cdot \mathcal{L}^{\text{SSIM}}(Y^{\text{pred}}, Y^{\text{GT}}) \tag{7}$$

where the weighting factor β is empirically set to 3.0 to balance the contributions from local and non-local loss terms.

The training of EMReady2 is conducted on two NVIDIA Tesla A100 GPUs with a batch size of 56. Adam optimizer is adopted to optimize the network through backpropagation. Learning rate is initially set to 2×10^{-4}, and will be reduced to half of its current value if the average loss on the training set does not decrease over 4 consecutive epochs. The training process continues until the learning rate reaches a minimum value of 10^{-6} or after 300 epochs on the training set. The choices of hyperparameters adopted by EMReady2 are based on empirical observations and computational efficiency. After each epoch on the training set, the model is applied to the validation set and the average loss on the validation set is calculated. The model that has the least loss on the validation set is selected to be used in the evaluation.

4.4 Evaluations of map quality and interpretability

We carry out comprehensive evaluations of EMReady2 on three different test sets. For each density map in these test sets, we first chunk it into overlapping volume slices of shape $48 \times 48 \times 48$ with a sliding stride of 12. Subsequently, these overlapping slices are fed into the selected EMReady2 model with the least validation loss. Finally, the resulting slices from the network are re-assembled into the output post-processed map and the overlapping sections are averaged.

Three programs are utilized to measure the quality of maps before and after post-processing. The first tool is phenix.mtriage[41], which is used to calculate the FSC-0.5 (the resolution at which the map-model Fourier shell correlation falls to 0.5). The second tool is MapQ plugin of UCSF Chimera, which reports Q-score[38]. Q-score measures the correlation between the density around each atom and a reference Gaussian density function. The third tool is phenix.map_model_cc[41], which reports three different real space correlation coefficients between the map and an ideal map generated from the atomic model: CC_box, CC_mask, CC_peaks. CC_box is calculated using the map values in

the entire map, CC_mask uses the map values inside a masked region around the atomic model, and CC_peaks only considers those high-density regions in the map.

In addition to the above map quality metrics, we also evaluate the performance of EMReady2 in improving map interpretability. For a fair evaluation, a *de novo* model building tool, phenix.map_to_model[11] is used to build the atomic models from the map regions segmented within 4.0 Å from each of the protein and nucleic acid chains in our first test set. Residue coverage and sequence recall, calculated by phenix.chain_comparison, are used to assess the accuracy of the built model of protein or nucleic acid relative to the PDB model. Protein residues are represented by $C\alpha$ atoms, while nucleic acid residues are represented by $C4'$ atoms. Residue coverage is the proportion of residues in the built model that have matched residues (distance within 3.0 Å) in the PDB model. Sequence recall is the number of the residues in the built model that have correct residue types compared to that of the PDB structure.

4.5 Comparison with related methods

EMReady2 is compared with state-of-the-art methods, including DeepEMhancer[30], phenix.auto_sharpen[26], and EMReady[32] on different test sets. For phenix.auto_sharpen and EMReady, default parameters are applied. For DeepEMhancer, which provides three different models: 'tightTarget', 'wideTarget', and 'highRes', we report the evaluation results in a combinatorial manner. Specifically, for cryo-EM SPA maps, we report the results from the "highRes" model for maps with resolutions higher than 4.0 Å, and report the results from the "tightTarget" model for maps with lower resolutions. For cryo-ET STA maps, due to their generally lower quality, we report the results from the "wideTarget" model.

Acknowledgments

This work was supported by the National Natural Science Foundation of China (grants No. 32161133002 and 62072199) and the startup grant of Huazhong University of Science and Technology.

Author contributions

S.H. conceived the project. S.H. and J.H. supervised the project. H.C. and J.H. implemented the methods and performed the experiments. H.C., J.H., T.L., and S.H. analyzed the data. H.C., J.H., T.L., and J.C. tested the program. H.C., J.H., and S.H. wrote the manuscript. All authors read and approved the final version of the manuscript.

Competing interests

The authors declare no competing interests.

Data availability

The raw data of the evaluation results are provided in the Article. All published data sets used in this paper were taken from the EMDB and PDB. Other data that support the study are available upon reasonable request from the corresponding author.

Code availability

The EMReady2 package is freely available for academic or non-commercial users at http://huanglab.phys.hust.edu.cn/EMReady2/.

References

(1) Li X, Mooney P, Zheng S, et al. Electron counting and beam-induced motion correction enable near-atomic-resolution single-particle cryo-EM. Nat Methods. 2013;10(6):584-590.

(2) Xu Y, Dang S. Recent Technical Advances in Sample Preparation for Single-Particle Cryo-EM. Front Mol Biosci. 2022;9:892459.

(3) de la Rosa-Trevín JM, Quintana A, Del Cano L, et al. Scipion: A software framework toward integration, reproducibility and validation in 3D electron microscopy. J Struct Biol. 2016;195(1):93-99.

(4) Punjani A, Rubinstein JL, Fleet DJ, Brubaker MA. cryoSPARC: algorithms for rapid unsupervised cryo-EM structure determination. Nat Methods. 2017;14(3):290-296.

(5) Zivanov J, Nakane T, Forsberg BO, et al. New tools for automated high-resolution cryo-EM structure determination in RELION-3. Elife. 2018;7:e42166. Published 2018 Nov 9.

(6) Vilas JL, Carazo JM, Sorzano COS. Emerging Themes in CryoEM-Single Particle Analysis Image Processing. Chem Rev. 2022;122(17):13915-13951.

(7) Chari A, Stark H. Prospects and Limitations of High-Resolution Single-Particle Cryo-Electron Microscopy. Annu Rev Biophys. 2023;52:391-411.

(8) Young LN, Villa E. Bringing Structure to Cell Biology with Cryo-Electron Tomography. Annu Rev Biophys. 2023;52:573-595.

(9) Nogales E, Mahamid J. Bridging structural and cell biology with cryo-electron microscopy. Nature. 2024;628(8006):47-56.

(10) Emsley P, Lohkamp B, Scott WG, Cowtan K. Features and development of Coot. Acta Crystallogr D Biol Crystallogr. 2010;66(Pt 4):486-501.

(11) Terwilliger TC, Adams PD, Afonine PV, Sobolev OV. A fully automatic method yielding initial models from high-resolution cryo-electron microscopy maps. Nat Methods. 2018;15(11):905-908.

(12) Terwilliger TC, Poon BK, Afonine PV, et al. Improved AlphaFold modeling with implicit experimental information. Nat Methods. 2022;19(11):1376-1382.

(13) He J, Huang SY. EMNUSS: a deep learning framework for secondary structure annotation in cryo-EM maps. Brief Bioinform. 2021;22(6):bbab156.

(14) He J, Huang SY. Full-length de novo protein structure determination from cryo-EM maps using deep learning. Bioinformatics. 2021;37(20):3480-3490.

(15) He J, Lin P, Chen J, Cao H, Huang SY. Model building of protein complexes from intermediate-resolution cryo-EM maps with deep learning-guided automatic assembly. Nat Commun. 2022;13(1):4066.

(16) Li T, He J, Cao H, et al. All-atom RNA structure determination from cryo-EM maps. Nat Biotechnol. Published online February 23, 2024. doi:10.1038/s41587-024-02149-8

(17) Zhou X, Li Y, Zhang C, Zheng W, Zhang G, Zhang Y. Progressive assembly of multi-domain protein structures from cryo-EM density maps. Nat Comput Sci. 2022;2(4):265-275.

(18) Zhang X, Zhang B, Freddolino PL, Zhang Y. CR-I-TASSER: assemble protein structures from cryo-EM density maps using deep convolutional neural networks. Nat Methods. 2022;19(2):195-204.

(19) Pfab J, Phan NM, Si D. DeepTracer for fast de novo cryo-EM protein structure modeling and special studies on CoV-related complexes. Proc Natl Acad Sci U S A. 2021;118(2):e2017525118.

(20) Jamali K, Käll L, Zhang R, Brown A, Kimanius D, Scheres SHW. Automated model building and protein identification in cryo-EM maps. Nature. 2024;628(8007):450-457.

(21) Vilas JL, Gómez-Blanco J, Conesa P, et al. MonoRes: Automatic and Accurate Estimation of Local Resolution for Electron Microscopy Maps. Structure. 2018;26(2):337-344.e4.

(22) Vilas JL, Tagare HD, Vargas J, Carazo JM, Sorzano COS. Measuring local-directional resolution and local anisotropy in cryo-EM maps. Nat Commun. 2020;11(1):55.

(23) Vilas JL, Tagare HD. New measures of anisotropy of cryo-EM maps. Nat Methods. 2023;20(7):1021-1024.

(24) Rosenthal PB, Henderson R. Optimal determination of particle orientation, absolute hand, and contrast loss in single-particle electron cryomicroscopy. J Mol Biol. 2003;333(4):721-745.

(25) Jakobi AJ, Wilmanns M, Sachse C. Model-based local density sharpening of cryo-EM maps. Elife. 2017;6:e27131.

(26) Terwilliger TC, Sobolev OV, Afonine PV, Adams PD. Automated map sharpening by maximization of detail and connectivity. Acta Crystallogr D Struct Biol. 2018;74(Pt 6):545-559.

(27) Ramírez-Aportela E, Vilas JL, Glukhova A, et al. Automatic local resolution-based sharpening of cryo-EM maps. Bioinformatics. 2020;36(3):765-772.

(28) Terwilliger TC, Ludtke SJ, Read RJ, Adams PD, Afonine PV. Improvement of cryo-EM maps by density modification. Nat Methods. 2020;17(9):923-927.

(29) Kaur S, Gomez-Blanco J, Khalifa AAZ, et al. Local computational methods to improve the interpretability and analysis of cryo-EM maps. Nat Commun. 2021;12(1):1240.

(30) Sanchez-Garcia R, Gomez-Blanco J, Cuervo A, Carazo JM, Sorzano COS, Vargas J. DeepEMhancer: a deep learning solution for cryo-EM volume post-processing. Commun Biol. 2021;4(1):874.

(31) Maddhuri Venkata Subramaniya SR, Terashi G, Kihara D. Enhancing cryo-EM maps with 3D deep generative networks for assisting protein structure modeling. Bioinformatics. 2023;39(8):btad494.

(32) He J, Li T, Huang SY. Improvement of cryo-EM maps by simultaneous local and non-local deep learning. Nat Commun. 2023;14(1):3217.

(33) Zhang K, Li Y, Liang J, et al. Practical blind denoising via swin-conv-unet and data synthesis. arXiv preprint. 2022. arXiv:2203.13278.

(34) Sonani RR, Sanchez JC, Baumgardt JK, et al. Tad and toxin-coregulated pilus structures reveal unexpected diversity in bacterial type IV pili. Proc Natl Acad Sci U S A. 2023;120(49):e2316668120.

(35) Liu C, Hauk G, Yan Q, Berger JM. Structure of Escherichia coli exonuclease VII. Proc Natl Acad Sci U S A. 2024;121(5):e2319644121.

(36) Wang H, Liu X, Zhang X, et al. TMPRSS2 and glycan receptors synergistically facilitate coronavirus entry. Cell. Published online June 21, 2024.

(37) Augestad EH, Holmboe Olesen C, Grønberg C, et al. The hepatitis C virus envelope protein complex is a dimer of heterodimers. Nature. Published online September 4, 2024.

(38) Pintilie G, Zhang K, Su Z, Li S, Schmid MF, Chiu W. Measurement of atom resolvability in cryo-EM maps with Q-scores. Nat Methods. 2020;17(3):328-334.

(39) Lawson CL, Patwardhan A, Baker ML, et al. EMDataBank unified data resource for 3DEM. Nucleic Acids Res. 2016;44(D1):D396-D403.

(40) Berman HM, Westbrook J, Feng Z, et al. The Protein Data Bank. Nucleic Acids Res. 2000;28(1):235-242.

(41) Afonine PV, Klaholz BP, Moriarty NW, et al. New tools for the analysis and validation of cryo-EM maps and atomic models. Acta Crystallogr D Struct Biol. 2018;74(Pt 9):814-840.

(42) Pettersen EF, Goddard TD, Huang CC, et al. UCSF Chimera–a visualization system for exploratory research and analysis. J Comput Chem. 2004;25(13):1605-1612.

(43) Steinegger M, Söding J. MMseqs2 enables sensitive protein sequence searching for the analysis of massive data sets. Nat Biotechnol. 2017;35(11):1026-1028.

(44) Paszke A, Gross S, Massa F, Lerer A, et al. PyTorch: An imperative style, high-performance deep learning library. In: Advances in Neural Information Processing Systems; 2019:32.

Table 1: Comparing the quality of the deposited and processed maps on a test set of 18 nucleic acid-included cryo-EM maps at 2–7 Å resolutions.

Method	FSC-0.5	Q-score	CC_box	CC_mask	CC_peaks
deposited	5.70	0.453	0.820	0.765	0.706
DeepEMhancer	4.94	0.368	0.665	0.637	0.616
phenix.auto_sharpen	5.70	0.446	0.702	0.704	0.582
EMReady	4.59	0.458	0.871	0.771	0.761
EMReady2	**4.18**	**0.501**	**0.883**	**0.786**	**0.765**

Table 2: Comparing the quality of the deposited and processed maps on a test set of 58 cryo-EM maps with resolutions ranging from 4 to 8 Å.

Method	FSC-0.5	Q-score	CC_box	CC_mask	CC_peaks
deposited	7.63	0.313	0.770	0.672	0.558
DeepEMhancer	7.11	0.203	0.602	0.549	0.497
phenix.auto_sharpen	7.63	0.307	0.695	0.640	0.490
EMReady	6.63	0.314	0.814	0.669	0.623
EMReady2	**6.36**	**0.331**	**0.838**	**0.696**	**0.633**

Table 3: Comparing the quality of the deposited and processed maps on the test set of 18 cryo-ET maps at 3-10 Å resolutions.

Method	Masked FSC-0.5	Q-score	CC_box
deposited	7.06	0.361	0.510
DeepEMhancer	6.83	0.280	0.471
phenix.auto_sharpen	6.92	0.364	0.461
EMReady	6.45	0.378	0.611
EMReady2	**6.32**	**0.392**	**0.642**

Table 4: Comparison of the map interpretability in terms of de novo model building on the test set of 18 EM maps processed by EMReady2 and four other methods. The test set include 74 protein chains and 37 nucleic acid chains.

Method	Residue coverage(%)		Sequence recall(%)	
	Protein	Nucleic acid	Protein	Nucleic acid
deposited	56.60	45.11	15.36	19.39
DeepEMhancer	50.82	39.54	16.98	15.50
phenix.auto_sharpen	57.36	50.18	16.82	18.91
EMReady	66.95	57.56	24.44	22.98
EMReady2	**69.44**	**68.32**	**28.60**	**24.57**

Figure 1

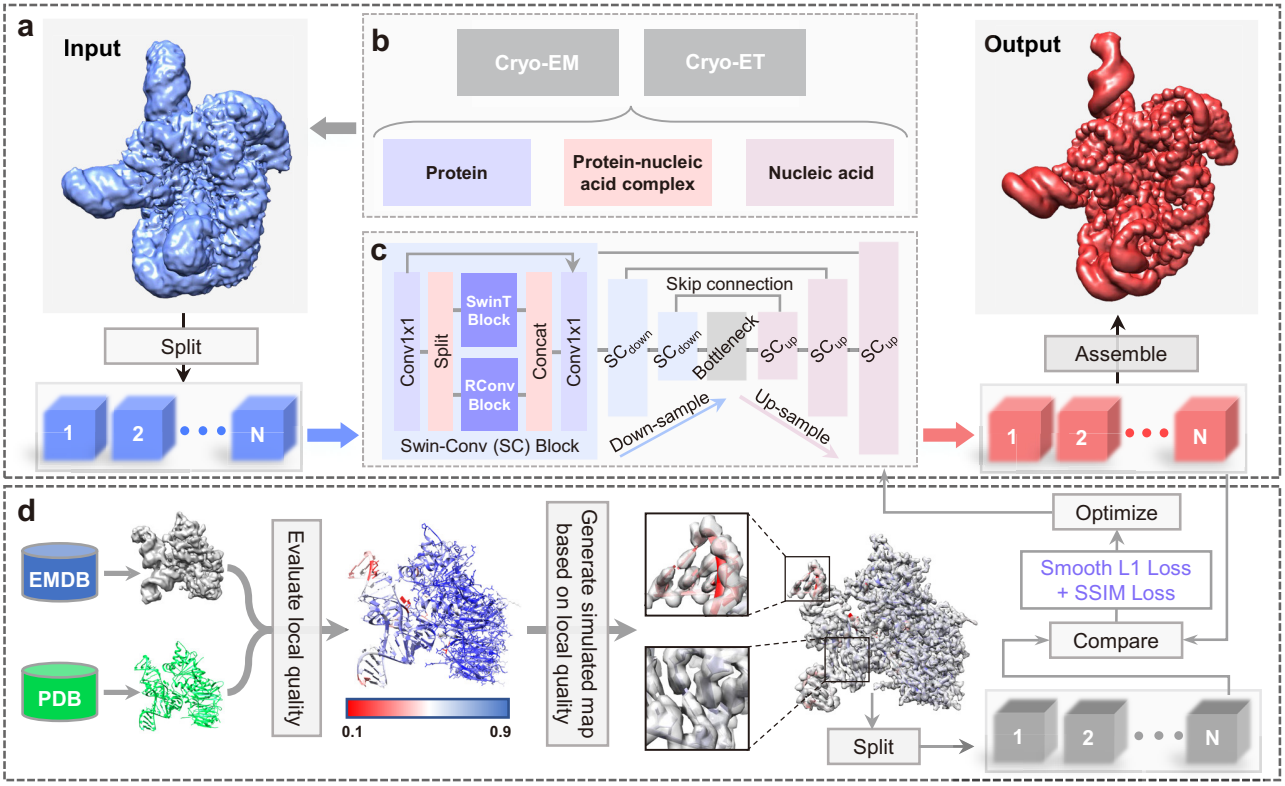

Figure 1: Overview of EMReady2. a–c, Post-processing workflow of EMReady2. The input for EMReady2 is an EM density map from cryo-EM SPA or cryo-ET STA, which may contain proteins, nucleic acids, or their complexes (**b**). The input density map is first chunked into a series of overlapping volume slices, which are then fed into a 3D SCUNet network[33] (**c**) to obtain the processed slices. These processed slices are re-assembled to yield the output post-processed map. **d**, Training workflow of EMReady2. A non-redundant set of pairs of experimental map and the associated atomic structure is obtained from the EMDB[39] and the PDB[40]. For each pair of atomic structure and its corresponding density map in the training set, a simulated density map is generated using different local resolutions derived from Q-scores[38] for different atoms. The experimental map and its corresponding simulated map are chunked into pairs of volume slices. In each training iteration, experimental volume slices are processed by the network and then compared with the corresponding simulated slices based on a combinatorial loss function of smooth L1 loss and SSIM loss, optimizing the network parameters.

Figure 2

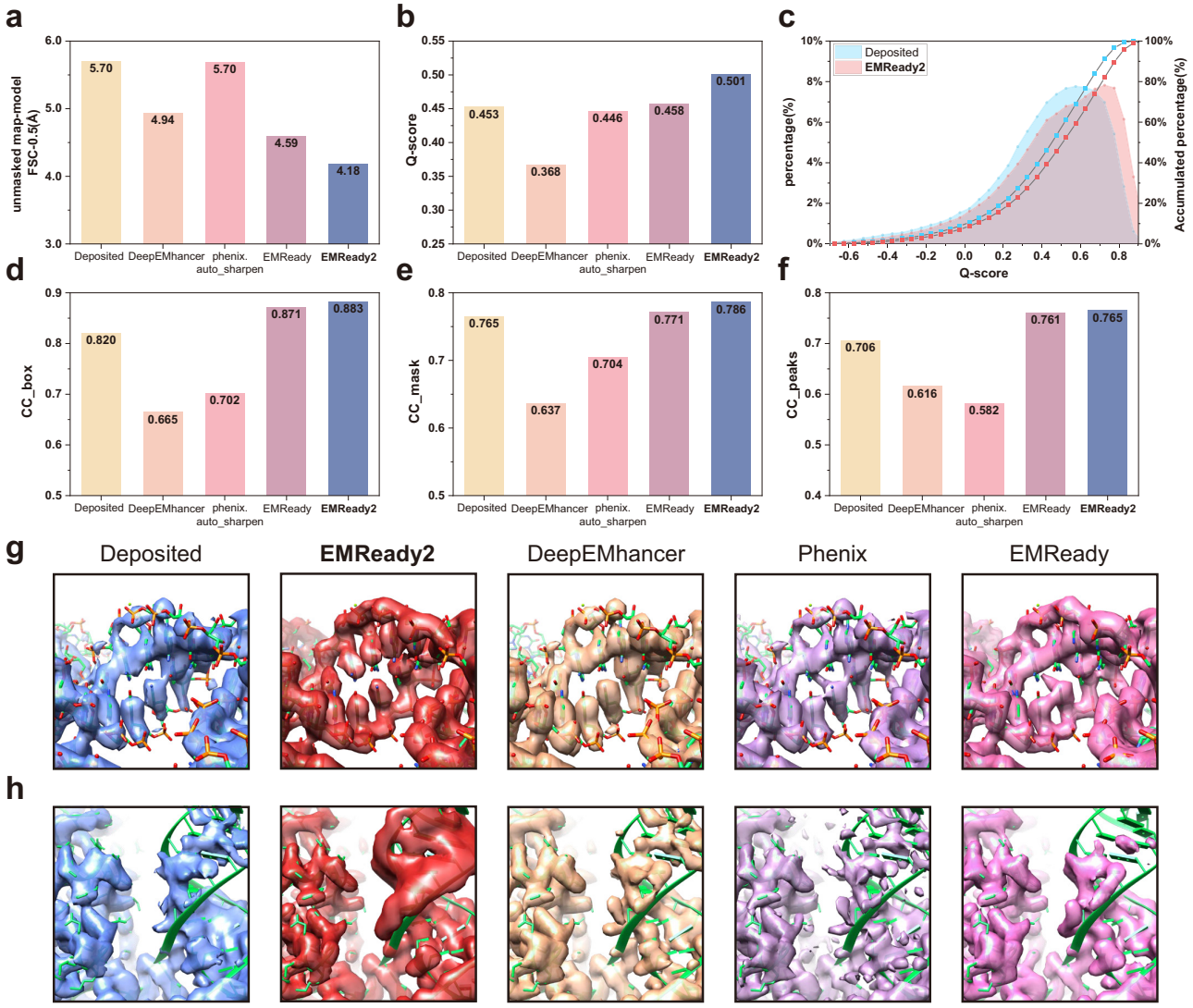

Figure 2: Evaluation results on the test set of 18 cryo-EM SPA maps containing nucleic acids at 2–7 Å resolutions. a,b,d–f, Comparison of average unmasked map-model FSC-0.5 resolutions (**a**), Q-scores (**b**), CC_box (**d**), CC_mask (**e**), and CC_peaks values (**f**) for the deposited, DeepEMhancer-processed, phenix.auto_sharpen-processed, EMReady-processed, and EMReady2-processed maps. **c**, Comparison of the distribution (Fill Area, left y-axis) and accumulated percentages (Line+Symbol, right y-axis) of Q-scores for nucleic acid atoms on the deposited and EMReady2-processed maps. **g-h**, Comparison of the deposited map and the processed maps by different methods for (**g**) EMD-9105 (associated PDB ID: 6ME0) at 3.60 Å resolution and (**h**) EMD-33983 (associated PDB ID: 7YOJ) at 3.36 Å resolution. Contours are drawn to enclose equal volumes for each case.

Figure 3

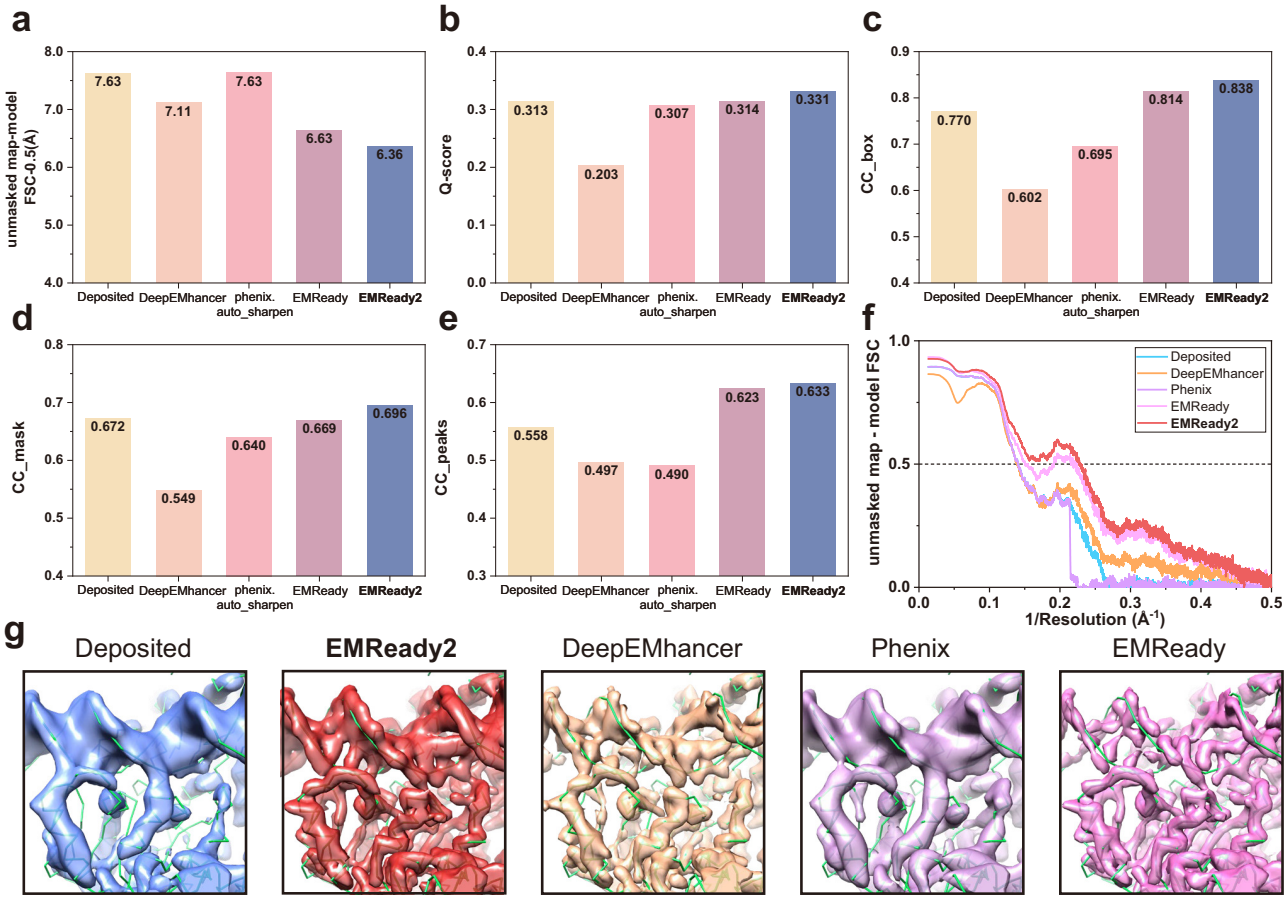

Figure 3: Evaluation results on the test set of 58 cryo-EM SPA maps at 4.0-8.0 Å resolutions. **a**–**e**, Comparison of average unmasked map-model FSC-0.5 resolutions (**a**), Q-scores (**b**), CC_box (**c**), CC_mask (**d**), and CC_peaks values (**e**) for the deposited, DeepEMhancer-processed, phenix.auto_sharpen-processed, EMReady-processed, and EMReady2-processed maps. **f**,**g**, Example of EMD-28000 (associated PDB ID: 8EBW) at 5.6 Å resolution: (**f**) Unmasked map-model FSC versus spatial frequency; (**g**) Comparison of the deposited map and maps post-processed by different methods. Contours are drawn to enclose equal volumes for each case.

Figure 4

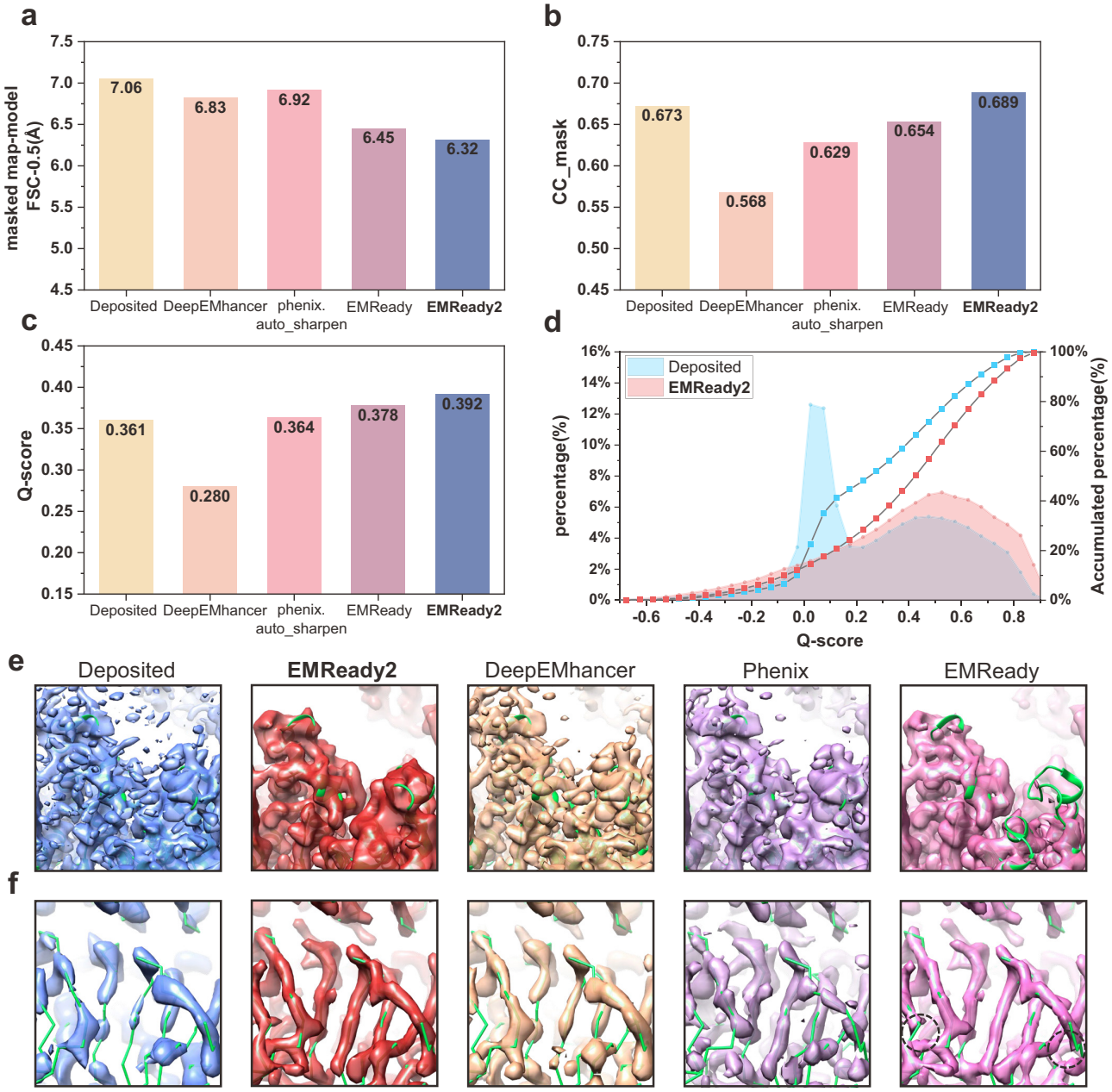

Figure 4: Evaluation results on the test set of 18 cryo-ET STA maps at 3–10 Å resolutions. a–c, Comparison of average masked map-model FSC-0.5 resolutions (**a**), CC_mask (**b**), and Q-scores (**c**) for the deposited, DeepEMhancer-processed, phenix.auto_sharpen-processed, EMReady-processed, and EMReady2-processed maps. **d**, Comparison of the distribution (Fill Area, left y-axis) and accumulated percentages (Line+Symbol, right y-axis) of Q-scores for atoms on the deposited map and on the EMReady2-processed map. **e-f**, Comparison of the deposited map the maps processed by different mthods for (**e**) EMD-12487 (associated PDB ID: 7NO2) at 4.30 Å resolution and (**f**) EMD-14617 (associated PDB ID: 7CZ1) at 3.80 Å resolution. Dashed circles indicate areas that are poorly post-processed by EMReady. Contours are drawn to enclose equal volumes for each case.

Figure 5

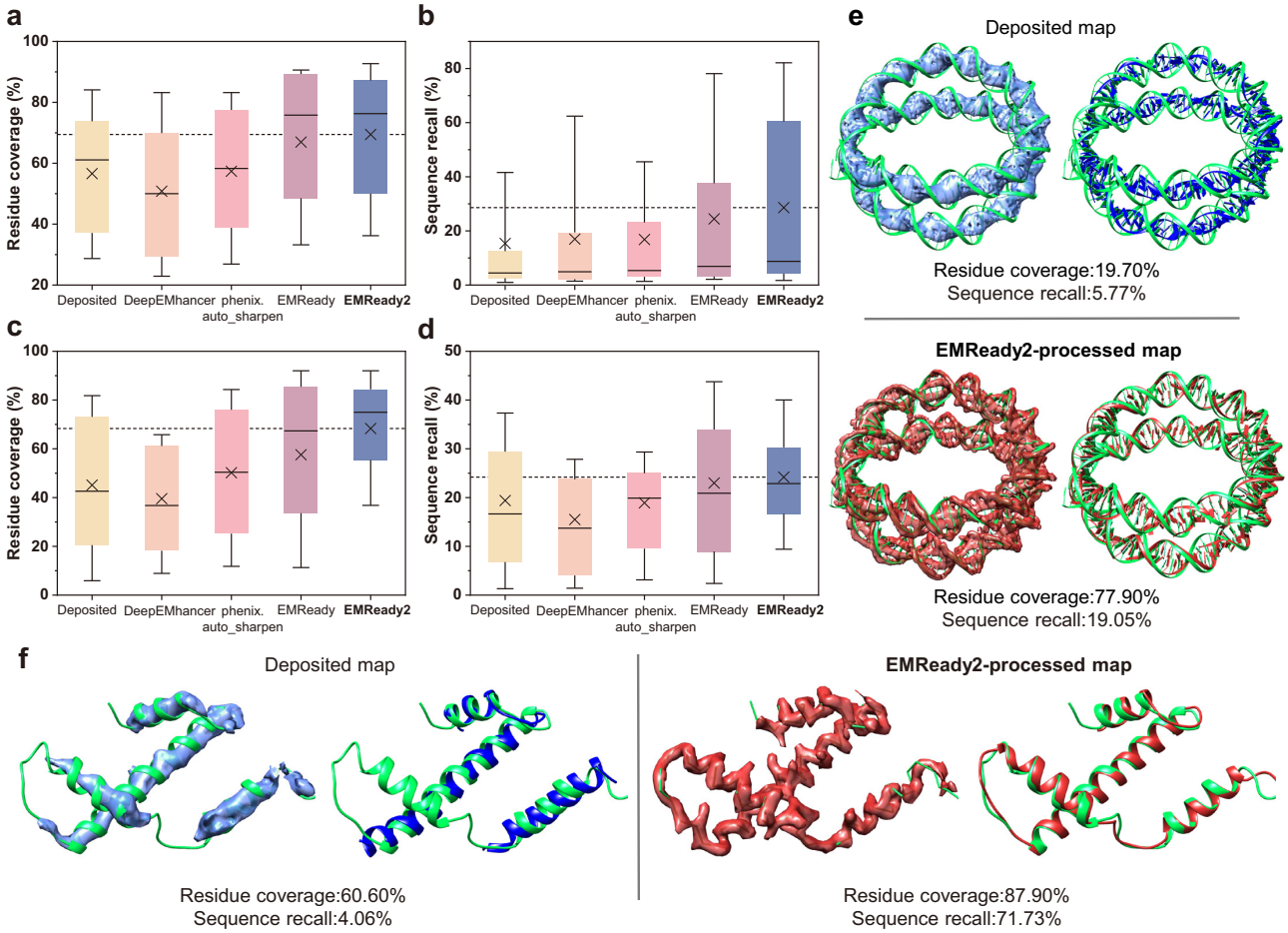

Figure 5: Improvement in map interpretability on the test set of 74 protein chains and 37 nucleic acid chains. a,b, Box-whisker plots of the residue coverage (**a**) and sequence recall (**b**) for the built models of 74 protein chains. **c,d**, Box-whisker plots of the residue coverage (**c**) and sequence recall (**d**) for the built models of 37 nucleic acid chains. The center line is the median, the cross is the mean, lower and upper hinges represent the first and third quartile, the whiskers stretch to 1.5 times the interquartile range from the corresponding hinge, and the outliers are plotted as diamonds. Dashed lines stand for the average values achieved by EMReady2. **e**, Chains I and J of 6R25 on EMD-4710 at 4.61 Å resolution. The upper and lower panels display the deposited and the EMReady2-processed maps and the corresponding built models, respectively. **f** Chain E of 6R25 on EMD-4710 at 4.61 Å resolution. The left and right panels display the deposited and the EMReady2-processed maps and their corresponding built models, respectively. The reference PDB structures are colored in green. The deposited maps and their corresponding models are colored in blue. The EMReady2-processed maps and their corresponding models are colored in red. Contours are drawn to enclose equal volumes for each case.

Figure 6

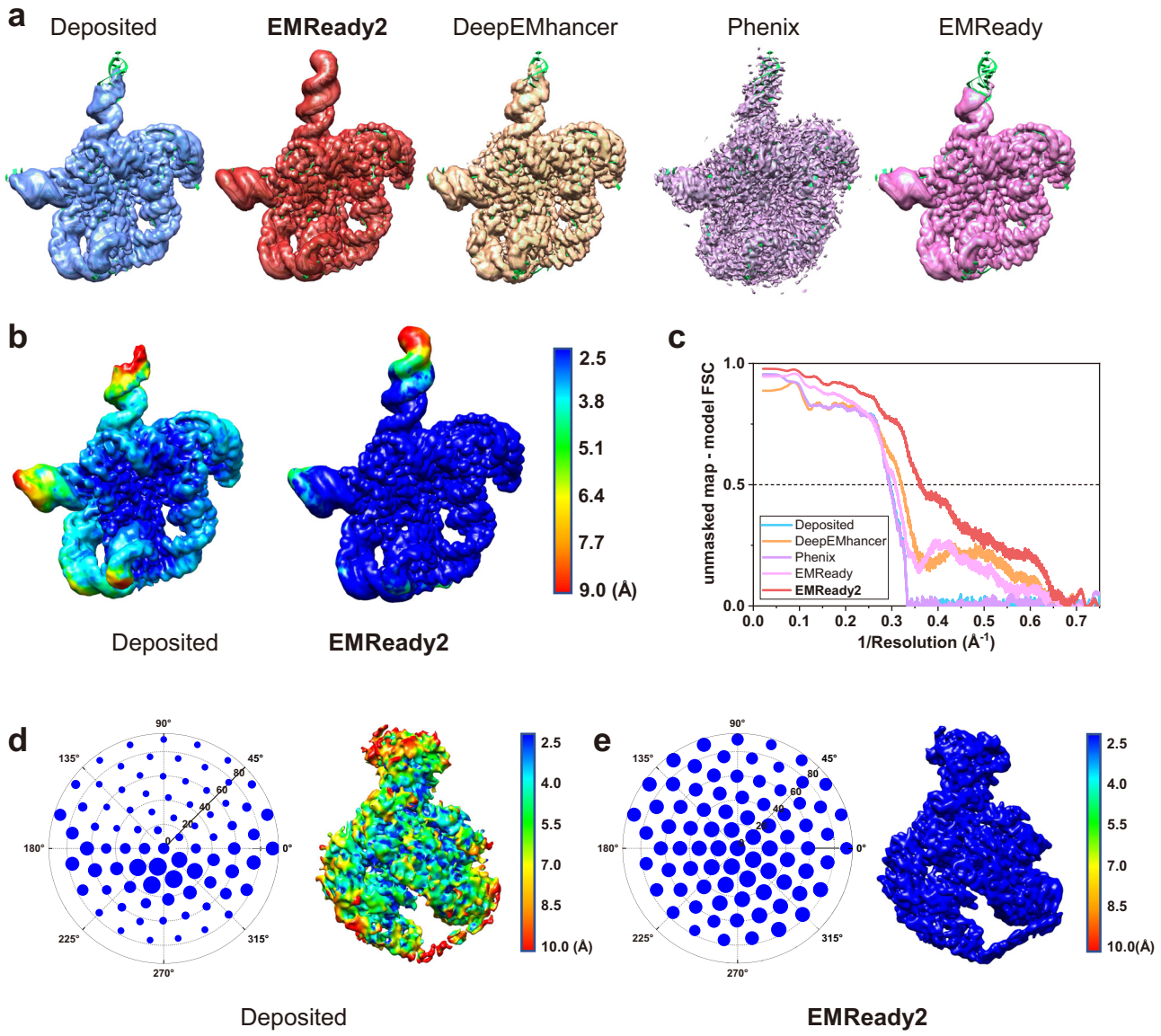

Figure 6: Robustness of EMReady2 against map heterogeneity. **a**–**c**, Example of EMD-33428 (associated PDB ID: 7XSN) at 3.01 Å resolution: (**a**) Comparison of the deposited map and maps post-processed by different methods; (**b**) Comparison of local resolution maps between the deposited map (left panel) and the EMReady2-processed map (right panel); (**c**) Unmasked map-model FSC versus spatial frequency. **d**,**e**, Example of EMD-20501 (associated PDB ID: 6PW9) at 4.03 Å resolution: (**d**) Local resolution map (left panel) and the angular plots for the local-directional resolution map (right panel) of the deposited map; (**e**) Local resolution map (left panel) and the angular plots for the local-directional resolution map (right panel) of the EMReady2-processed map. Contours are drawn to enclose equal volumes for each case.